Riparian vegetation limits oxidation of thermodynamically unfavorable bound-carbon stocks along an aquatic interface

Emily B. Graham[1], Malak Tfaily[2], Alex R. Crump[1], Amy E. Goldman[1], Evan Arntzen[1], Elvira Romero[1], C. Tom Resch[1], David W. Kennedy[1], and James C. Stegen[1]

[1]Pacific Northwest National Laboratory, Richland, WA USA

[2]Environmental Molecular Science Laboratory, Richland, WA USA

Correspondence: Emily B. Graham, Pacific Northwest National Laboratory, PO Box 999, Richland, WA 99352, 509-372-6049, emily.graham@pnnl.gov

Keywords: terrestrial, priming, recalcitrant, labile, FT-ICR, Hanford, KEGG, respiration

In light of increasing terrestrial carbon (C) transport across aquatic boundaries, the mechanisms governing organic carbon (OC) oxidation along terrestrial-aquatic interfaces are crucial to future climate predictions. Here, we investigate biochemistry, metabolic pathways, and thermodynamics corresponding to OC oxidation in the Columbia River corridor. We leverage natural vegetative differences to encompass variation in terrestrial C inputs. Our results suggest that decreases in terrestrial C deposition associated with diminished riparian vegetation induce oxidation of physically-bound (i.e., mineral and microbial) OC at terrestrial-aquatic interfaces. We also find that contrasting metabolic pathways oxidize OC in the presence and absence of vegetation and—in direct conflict with the concept of 'priming'—that inputs of water-soluble and thermodynamically-favorable terrestrial OC protects bound-OC from oxidation. Based on our results, we propose a mechanistic conceptualization of OC oxidation along terrestrial-aquatic interfaces that can be used to model heterogeneous patterns of OC loss under changing land cover distributions.

Soils and nearshore sediments comprise a C reservoir that is 3.2 times larger than the atmospheric C pool[1], yet Earth System Models (ESMs) struggle to integrate mechanisms of OC oxidation into predictions of atmospheric carbon dioxide concentrations[2-4]. In particular, OC oxidation in nearshore habitats constitutes a significant uncertainty in atmospheric C flux[5,6] and knowledge on C cycling along these transition ecosystems is necessary to accurately predict global C cycling[1]. Terrestrial C inputs into aquatic systems have nearly doubled since pre-industrial times; an estimated 2.9 Pg C now crosses terrestrial-aquatic interfaces annually (vs. 0.9 Pg C yr^{-1} stored within forested ecosystems)[7,8]. The magnitude of this flux has garnered significant recent attention[5,7,8], yet the biochemical, metabolic, and thermodynamic mechanisms governing OC oxidation along aquatic interfaces remain a crucial uncertainty in climate predictions. New molecular techniques are providing insight into OC dynamics[9-11], but we still lack an understanding of why some OC remains stabilized for millennia whereas other OC is rapidly oxidized[12].

The ability of microorganisms to oxidize complex OC is an important constraint on C cycling, as OC is a mixture of compounds with different propensities for biotic oxidation[13,14]. Within terrestrial research, OC oxidation is often framed within the concept of ‘priming’, whereby microbial oxidation of chemically-complex and thermodynamically unfavorable OC is fueled by the addition of more bioavailable OC compounds[15]. However, the applicability of priming in aquatic environments is unclear[16-18]. Aquatic systems, and in particular nearshore environments, frequently experience mixing of terrestrial and aquatic C sources with distinct chemical character, providing a theoretical basis for priming expectations[16,17]. Consistent with priming, Guenet et al.[16] have proposed that this mixing generates “hotspots” or “hot moments” of biological activity facilitated by complementary C resources. Alternatively, OC stabilization in

sediments is tightly linked to organomineral interactions, which provide physical protection from extracellular enzyme activity[19-21], and the strength of these interactions may override any evidence for priming. Early investigations of priming effects in aquatic systems have been inconclusive, with evidence both for[22] and against[17,23] priming mechanisms.

Several new perspectives have attempted to move beyond frameworks such as priming that depend on strict chemical definitions to predict OC oxidation[1,24,25]. Two recent perspectives propose that the probability of OC oxidation is related to a spectrum of chemical properties and that even very complex OC can be oxidized when more favorable OC is depleted or isolated from microorganisms. Lehmann and Kleber[25] have proposed a 'soil continuum hypothesis' whereby OC is a gradient of continuingly decomposing compounds that are variably accessible for biotic oxidation, with no notion of chemically labile versus recalcitrant compounds. Similarly, Burd et al.[1] have suggested that OC oxidation is a 'logistical problem' involving the ability of microorganisms to access and metabolize compounds. Both concepts capture the emerging belief that chemically-complex, thermodynamically unfavorable OC can be oxidized when more favorable compounds are inaccessible.

Here, we address a critical knowledge gap in predicting the global C balance[1,5,6,8]—mechanisms governing OC oxidation along terrestrial-aquatic interfaces. Specifically, we investigate the biochemistry, microbial metabolism, and thermodynamics of OC oxidation in nearshore water-soluble and physically-bound (i.e., mineral and microbial) OC pools. We leverage natural variation in riparian vegetation along the Columbia River in Eastern Washington State (approximately 46° 22' 15.80"N, 119° 81 16' 31.52"W), the largest river in the U.S. west of the Continental Divide[26,27], to examine these mechanisms in the context of spatial variation in terrestrial C deposition. Vertical profiles were collected at three positions along each of two

transects—within patches of shoreline with or without riparian vegetation (hereafter, R and NR for 'riparian' and 'non-riparian', Table 1)—that ran perpendicular to river flow. Consistent with the priming paradigm and the presence of complementary resources in nearshore environments with terrestrial vegetation, we hypothesize that (a) C deposition associated with riparian vegetation increases total aerobic metabolism and enhances oxidation of bound-OC stocks, while (b) areas without riparian vegetation foster lower rates of aerobic metabolism with minimal oxidation of bound-OC.

Results.

Shifts in physicochemical, metabolic, and C character between vegetation states.

Differences in vegetation states (i.e., vegetated vs. unvegetated areas) between the transects corresponded to differences in physicochemistry, aerobic metabolism, and OC pool composition. R was characterized by mature trees (*Morus rubra* (Red Mulberry) and *Ulmus rubra* (Slippery Elm) with a closed canopy) near the water line and was nutrient-rich as compared to NR (Supplementary Fig. 1-3). R displayed comparatively high concentrations of total C and rates of aerobic metabolism (Supplementary Fig. 1-3). In contrast, NR consisted of vegetation-free, cobble-ridden shoreline with sandier soils, low total C, and low aerobic metabolism (Supplementary Fig. 1-3).

The composition of OC pools was also distinct at each vegetation state (Fig. 1). We evaluated OC composition by sequential water- (H_2O), methanol (-MeOH), and chloroform- ($CHCl_3$) extractions[10,11], followed by analysis via Fourier transform ion cyclotron resonance mass spectrometry (FT-ICR-MS). Previous work has shown that each solvent is selective towards the type of compounds it extracts[10]. Because MeOH has a polarity in between that of

water and $CHCl_3$, it extracts both water-soluble and bound-OC pools (i.e., a mix of compounds that water and $CHCl_3$ extract). In this study we are interested in the differences in OC composition between pure water-soluble and bound-OC pools only, and we will focus our discussion on H_2O- and $CHCl_3$-extractions only. Water is a polar solvent with a selection bias for carbohydrates with high O/C ratios, amino-sugars and other labile polar compounds[10]; and, as nearshore environments frequently experience wetting, water extractions represents an estimation of physically accessible OC compounds in these environments. Conversely, $CHCl_3$ is selective for non-polar lipids associated with mineral interactions and cellular membranes[10]. We use H_2O- and $CHCl_3$-extracted OC as proxies for readily bioavailable (i.e., weakly bound physically) vs. less bioavailable (i.e., mineral-bound and microbial) pools, respectively.

Compositional difference in OC pools indicated a possibility for fundamentally different OC oxidation processes at each vegetation state, whereby preferential oxidation of certain compounds was either driven by or generates an observable difference in OC pool composition. Further, total organic OC content explained only 38% of aerobic metabolism rates ($R^2 = 0.38$, $P < 0.0001$, Supplementary Fig. 4), leaving open the possibility that OC compositional differences may be related to differences in aerobic metabolism at each vegetation state.

Associations between C transformations and aerobic metabolism.

Given chemical differences across vegetation states in each OC pool and known impacts of C chemistry on metabolic functioning in other systems[28,29], we postulated that compound-specific transformations may be related to rates of aerobic metabolism at each of our vegetation states. To reveal transformations associated with aerobic metabolism—and to study differences in those transformations across vegetation states—we estimated the number of times a given

transformation occurred within each OC pool, within each sample. In turn, these 'abundance' estimates were correlated to rates of metabolism (resazurin assay, see Methods). Transformations were identified as mass differences in known biochemical pathways between peaks detected by FT-ICR-MS (i.e., the mass gained or lost in reactions, see Methods, Fig. 2). Positive relationships were inferred as processes possibly associated with biotic OC oxidation. We refer to H_2O- and $CHCl_3$-soluble OC pools at R and NR, respectively, as RW ('riparian water'), RC ('riparian chloroform'), NRW ('non-riparian water'), and NRC ('non-riparian chloroform') for the remainder of the manuscript.

Transformation analysis indicated that the biochemical processes associated with OC oxidation are significantly different across riparian vegetation conditions. Specifically, the identities of OC transformations that increased in abundance with increases in aerobic metabolism at each vegetation state were significantly different (PERMANOVA, H_2O $P = 0.022$ and $CHCl_3$ $P = 0.002$, Fig. 3 a-b, Table 2). In comparing differences in transformations occurring with the water-soluble OC pool, we observed a dominance of amino- and sugar-associated transformations at RW vs. NRW. Twenty-six transformations were identified as contributing to aerobic metabolism in RW, while none were identified in NRW. These RW transformations were primarily associated with glucose, alanine, and lysine (Table 2). Conversely, within the bound-OC pool, 38 transformations were identified as contributing to aerobic metabolism in NRC, compared to only 11 in RC. In both cases, these transformations consisted of complex C molecules such as pyridoxal phosphate, palmitic acid, and glyoxylate (Table 2).

The larger number of transformations associated with aerobic metabolism in NR vs. NRW, and the larger number in NRC vs. NW, suggests that aerobic metabolism in vegetated and unvegetated areas depend on water-soluble and bound-OC pools, respectively. We note some

oxidation of the bound-OC pool under vegetated conditions, but only 11 correlations were observed between RC transformations and aerobic metabolism suggesting a relatively minor role, especially considering that there were 38 significant correlations for NRC. This evidence suggests that an increased supply of bioavailable compounds in vegetated areas leads to bound-OC being less involved in aerobic metabolism, relative to unvegetated areas where bound-OC appears to be heavily involved in aerobic metabolism. The concept of priming[15] would predict the opposite pattern—a greater supply of bioavailable OC should increase the contributions of less bioavailable OC (here, bound-OC) to aerobic metabolism. Our results run counter to a priming mechanism and indicate that the supply of bioavailable compounds—associated with riparian vegetation—diminishes the contribution of bound-OC to aerobic metabolism and, in turn, protects bound-OC pools. Mineral-stabilized OC therefore has greater potential to remain sequestered along river corridors with spatially and temporally consistent inputs of bioavailable OC, potentially derived from riparian vegetation. The fate of OC that moves across the terrestrial-aquatic continuum in may be impacted by land use change[30] in ways not currently represented in ESMs.

Associations between microbial metabolic pathways and aerobic metabolism.

Across vegetation conditions we observed stark differences in the identity of C transformations that correlated with aerobic metabolic rate. In turn, we hypothesized that the microbial metabolic pathways associated with OC transformations were also dependent on vegetation condition. To address this hypothesis, we first identified the FT-ICR-MS peaks involved in the molecular transformations that were correlated with metabolic rate; each instance of each transformation involves two peaks (a reactant and a product). These peaks were mapped

to microbial metabolic pathways represented in Kyoto Encyclopedia of Genes and Genomes (KEGG, see Methods, Fig. 2)[31]. Like the previous section, we correlated the abundance of these pathways within each sample to aerobic metabolism and inferred positive correlations as microbial metabolic pathways contributing to OC oxidation. Results were visualized with a hierarchical clustering heat map based on relative abundance of each pathway contributing to OC oxidation (See Methods, Fig 4).

Pathways associated with OC oxidation were distinct at R vs. NR, further supporting our hypothesis that there were fundamental differences in the metabolic processing of OC in the presence or absence of riparian vegetation. Specifically, while the metabolism of plant-derived compounds appeared to be a major driver of aerobic respiration at both vegetation states, metabolism at R mostly involved the readily bioavailable plant derivatives in the H_2O-soluble OC pool, and metabolism at NR was associated with plant derivatives in the $CHCl_3$-soluble pool (Fig. 4).

In RW, two primary pathways were involved in metabolism of plant compounds, each contained within its own hierarchical cluster (map01110: Biosynthesis of secondary metabolites; map00941: Flavonoid biosynthesis). A concomitant cluster of plant-associated metabolisms in RW (Cluster 4) was also positively correlated to aerobic metabolism (Fig. 4). Secondary metabolites (map01110) are largely comprised of plant-derived compounds such as flavonoids[32], terpenoids[33], and nitrogen-containing alkaloids[34], while flavonoids[32] are one of those most abundant plant-derived compounds. Associations with aflatoxin[35], flavone/flavonol[32], and phenylpropanoids[36] (Cluster 4) bolster this association between plant-associated metabolic pathways and aerobic metabolism in RW. Although correlations between plant-based KEGG pathways and aerobic metabolism could indicate the persistence of plant secondary metabolites

rather than microbial metabolism, our results indicate a central role for vegetation in water-soluble OC oxidation in either case. For example, if KEGG associations were attributable to plant metabolism instead of microbial metabolism, correlations between plant-associated KEGGs and aerobic metabolism in RW would indicate an indirect relationship between plant growth and microbial oxidation of OC, whereby plant byproducts support microbial communities in oxidizing other portions of the OC pool.

In contrast to RW, NRW did not display associations between plant-associated metabolic pathways and OC oxidation. All correlations indicated broad metabolic processes including membrane transport and carbohydrate metabolism that may indicate utilization of other resources (Cluster 3, Fig. 4).

Instead, we observed relationships between plant-associated metabolisms and OC oxidation within NRC. For example, correlations were strongest in Cluster 1, which contained pathways of cutin, suberine, and wax biosynthesis[37-39], alpha-linolenic acid metabolism[40,41], and biosynthesis of secondary metabolites[32-34] (Fig. 4). Each of these pathways denotes the synthesis or metabolism of a plant-associated lipid compound. Because no specific metabolisms were correlated to OC oxidation in the H_2O-soluble pool, we hypothesize that these lipid-based metabolisms comprise the primary KEGG-identifiable pathways associated with OC oxidation in areas without riparian vegetation. We also observed one cluster of pathways that correlated with metabolism at RC (Cluster 7) and contained plant-associated metabolic pathways such as linoleic acid metabolism[40,41] and brassinosteroid biosynthesis[42], indicating some oxidation of lipid plant material in the bound-OC pool under vegetated conditions. We therefore propose that plant-derived lipid compounds serve as a secondary substrate for OC oxidation in shorelines with riparian vegetation, given that most correlations at R were detected in the water-soluble pool.

Thermodynamics of carbon oxidation.

Finally, we hypothesized that microbes would preferentially oxidize more thermodynamically-favorable compounds at both sites, consistent with universal thermodynamic constraints on biogeochemical cycles[43-45]. Because we observed evidence for preferential OC oxidation in the water-soluble OC pool at R and in the bound-OC pool at NR, we further predicted that these constraints would be limited to oxidation of preferred substrate pools within each vegetation state. We determined Gibbs Free Energy of C oxidation (ΔG_{Cox}) of each OC pool via the stoichiometry of major elements in C compounds as per La Rowe and Van Cappellen[46]. ΔG_{Cox} is generally positive, indicating that C oxidation must be coupled to the reduction of a terminal electron acceptor for a thermodynamically favorable reaction, and higher ΔG_{Cox} denotes a less thermodynamically favorable compound, assuming consistency in the terminal electron acceptor. Then, we correlated rates of aerobic metabolism to ΔG_{Cox} in RW, RC, NRW, and NRC to reveal how thermodynamic favorability varied with the oxidation of each OC pool.

Aerobic metabolism positively correlated to ΔG_{Cox} in RW ($R^2 = 0.22$, $P = 0.03$, Fig 5a) and NRC ($R^2 = 0.54$, $P = 0.001$ Fig 5b) but did not correlate in RC or NRW. In both cases, aerobic metabolism corresponded to a depletion of more thermodynamically-favorable OC (i.e., OC became less favorable as aerobic metabolism increased), resulting in progressively unfavorable thermodynamic conditions.

The priming conceptual framework would predict that terrestrial inputs associated with riparian vegetation should condition microbial communities to oxidize less thermodynamically-favorable C, such as that found in the bound-OC pool. In such a scenario, inputs of

thermodynamically-favorable carbon should—by minimizing community-level energy constraints—allow for the rise of microbial physiologies that can oxidize less favorable C[15]. In this case, a significant relationship between thermodynamic favorability and aerobic metabolism in the RW pool should lead to a relationship within the RC pool. Our results reveal a strong relationship within the RW pool, but not in the RC pool, thereby rejecting an influence of priming. Instead, our results suggest that bound-OC pools are protected by thermodynamically-favorable compounds that serve as preferred substrate.

Discussion.

In contrast to our expectation that water-soluble OC associated with riparian vegetation would increase oxidation of bound-OC pools, we observed evidence consistent with inhibition of bound-OC oxidation by thermodynamically favorable water-soluble compounds. Priming has been actively debated in aquatic research[16-18], and a number of other studies have been unable to detect a priming effect in both sediment and aqueous habitats[17,23]. The mechanisms resulting in priming are not well understood, but the phenomenon has been associated with nutrient and energy limitations in soil environments[15]. For instance, under nutrient limitation, microorganisms may oxidize chemically-complex OC to garner resources (e.g., nitrogen mining), while shared resources that facilitate OC oxidation (e.g., extracellular enzymes) are more likely to facilitate ecological cheating under energy limiting conditions[15,16,23,47]. Our system is oligotrophic, containing a fraction of the total C content observed in other systems (Supplementary Fig. 1), and therefore, C limitation rather than nutrient limitation might drive OC oxidation dynamics. In such a case, readily bioavailable C inputs would be rapidly oxidized but microbial communities

may be well-adapted to rely on alternative energy sources (e.g., NH_4^+, Fe) that may be more available than bound-OC pools.

Conceptual model for OC oxidation at terrestrial-aquatic interfaces.

Based on our work, we propose a conceptual model of OC oxidation along terrestrial-aquatic interfaces in which the oxidation of bound-OC is limited by terrestrial inputs from riparian vegetation (Fig 6. a-b). Riparian vegetation sustains inputs of water-soluble compounds to nearshore OC pools, resulting in a larger thermodynamically-favorable and water-soluble OC pool (Fig. 6b). This leads to higher overall C content in nearshore sediments and elevated rates of aerobic respiration relative to low vegetation areas. However, microbial activity primarily operates on the water-soluble OC pool with minimal oxidation of bound-OC due to physical and/or thermodynamic protection of this pool. For instance, ΔG_{Cox} was higher in water-soluble OC pools than in bound-OC, and a large presence of this thermodynamically-favorable pool may provide adequate substrate to sustain metabolic functioning, limiting the need to metabolize less thermodynamically-favorable OC. Additionally, organomineral interactions physically protect OC from extracellular enzyme acitivity[19] and may require different enzymes than water-soluble OC, inhibiting the bioavailability of thermodynamically-favorable OC by sequestering it within larger aggregates.

In contrast, non-vegetated riparian zones provide little input into water-soluble OC pools (Fig 6a), and rates of metabolism and C pool sizes are lower in these environments. Carbon oxidation in these non-vegetated zones occurs primarily within the bound-OC pool, albeit more slowly and as product of different biochemical and metabolic pathways than in vegetated environments (e.g., complex C transformations and lipid-based metabolism of plant derivatives).

We posit that water-soluble pools in non-vegetated sediments are sufficiently small that investing in enzymes needed to metabolize this OC pool results in a net loss on energy investment. Instead, microbes in unvegetated areas must investment in cellular machinery to access bound-OC, and our results imply that the cellular machinery needed to access bound-OC is distinct from the machinery needed to access water-soluble OC.

Interestingly, aerobic metabolism within both types of sediments is related to a depletion of thermodynamically favorable compounds; however, this dynamic is associated with water-soluble OC pools in vegetated zones vs. bound-OC pools in non-vegetated zones. That is, microorganisms in both environments are constrained to the metabolism of their primary substrate pool but preferentially digest more energetically favorable compounds within that pool. This dynamic seems to suggest that microorganisms are conditioned to metabolize a subset of compounds within sediment OC, possibly defined by thermodynamic or physical protection mechanisms, but operate under universal thermodynamic constraints once adapted to oxidize a certain OC pool.

Broader Implications.

Our results indicate that terrestrial C inputs associated with riparian vegetation protect bound-OC from oxidation, possibly aiding long-term storage of mineral-bound pools along river corridors, and our work is particularly relevant to global patterns of CO_2 emissions in light of changes in land cover and increases in terrestrial-aquatic C fluxes. The magnitude, distribution, and chemical quality of terrestrial C fluxes into aquatic environments are perturbed by shifts in land cover (e.g., due to agriculture, urbanization, and climate-driven vegetation change)[48,49]. These fluxes have been examined primarily for their own propensity to be oxidized along land-

to-sea continuums[5,7,8], but we also suggest a role for these fluxes in stabilizing mineral-bound carbon within nearshore environments. For example, vegetation removal, impervious surfaces, and drainage systems coincident with urbanization alter terrestrial C runoff patterns, both increasing their magnitude and creating preferential deposition flowpaths[50-52]. Agricultural drainage systems also lead to preferential flowpaths as well as spatiotemporal variation in the quantity and quality of terrestrial-aquatic fluxes[53,54], an effect that strongly influences C cycling given that 40% of the earth's land is cultivated[30,53]. We propose that changes in the distribution of these fluxes through space and time may impact OC oxidation both in the C transported along these flow paths and within sediments that are differentially exposed to terrestrial OC.

Finally, vegetation distributions in natural ecosystems are predicted to shift in response to altered precipitation regimes. Associated changes in plant phenology, morphology, and establishment will impact the quantity, quality, and distribution of terrestrial material entering aquatic systems[49], and we currently have an incomplete understanding of how these patterns will vary across ecosystems and precipitation patterns[48,49]. A mechanistic framework for C oxidation along vegetative heterogeneity in river corridors will therefore aid in predicting how terrestrial-aquatic interfaces respond under proposed scenarios. Here, we demonstrate a potential for increases in the intensity of terrestrial C fluxes to lead to larger mineral-bound C pools by physically and thermodynamically protecting these pools; and conversely, a potential for oxidation of mineral-bound C pools in areas with diminished terrestrial C inputs.

Conclusions.

Earth System Models depend on mathematical representations of C cycling, and the continued development of these models is tightly coupled to conceptual advances drawn from

field-based observations[1,55]. Despite recent progress, these models are still missing key regulatory processes[2-4]. To address this knowledge gap, we propose a new model of OC dynamics based on analysis of *in situ* observational data that explicitly considers a central challenge in model improvement—biochemical, metabolic, and thermodynamic mechanisms governing OC oxidation along terrestrial-aquatic interfaces. Our results directly contrast those expected within a 'priming' framework, and we advance that water-soluble thermodynamically-favorable OC associated with riparian vegetation protects thermodynamically-unfavorable bound-OC from oxidation. We also demonstrate differences in biochemical and metabolic pathways associated with metabolism of water-soluble and bound-OC pools in the presence or absence of riparian vegetation, furthering a processed-based understanding of terrestrial-aquatic interfaces.

Our conceptualization of OC oxidation may also be applicable beyond terrestrial-aquatic interfaces, as many ecosystems experience spatiotemporal variability in the quantity of thermodynamically-favorable water-soluble OC. For instance, vegetation senescence generates pulses of bioavailable C into most temperate and tropical ecosystems. Our research provides an opportunity to enhance the mechanistic underpinning of OC oxidation process representations within ESMs—an imperative under heterogeneous landscapes and unknown future land cover distributions—and proposes interactions between OC thermodynamics and mineral-inhibition of OC oxidation as a key future research need.

Methods.

Site Description.

This study was conducted along the Columbia River shoreline within the Hanford 300A (approximately 46° 22’ 15.80”N, 119° 16’ 31.52”W) in eastern Washington State[56-58]. The Columbia River experiences shoreline geographic variation in vegetation patterns, substrate geochemistry, and microbiome composition[56,57,59-63]. Accordingly, the Hanford Reach of the Columbia River embodies a dynamic natural system in which to examine heterogeneity of terrestrial OC inputs and subsequent OC cycle mechanisms.

Liquid N_2-frozen sediment profiles (0-60 cm) were collected at two transects perpendicular to the Columbia River in March 2015, separated by a distance of ~170m. The southern transect (R) was characterized by a moderately sloping scour zone, small boulders; and vegetation consisted of woody perennials *Morus rubra* (Red Mulberry) and *Ulmus rubra* (Slippery Elm), with a closed canopy. Upper elevation samples were collected within the root zone. In contrast, the northern transect (R) was characterized by a gradually sloping scour zone and cobbled armor layer. Although a Red Mulberry was located nearby, the upper elevation samples were outside the root zone. We collected profiles at three locations in each transect with 5m spacing. The samples were collected as *in situ* liquid-N_2 frozen sediment profiles within a spatial domain of ~175 x 10m. In each transect, the first vertical profile (elevation 1) was located at ~0.5m (vertical distance) below the water line and the last vertical profile (elevation 3) was located ~0.5m (vertical distance) above the water line approximately 10m horizontal distance, with elevation 2 situated at the midpoint.

Sample Collection.

Liquid N_2-frozen sediment profiles were collected as outlined in Moser et al[27] using a method developed by Lotspeich and Reed[64] and modified by Rood and Church[65]. A pointed

stainless steel tube (152 cm length, 3.3 cm outside diameter, 2.4 cm inside diameter) was driven into the river bed to a depth of ~60cm. N_2(l) was poured down the tube for ~15 minutes, until a sufficient quantity of material had frozen to the outside of the rod. The rod and attached material was removed from the river bed with a chain hoist suspended beneath a tripod. Profiles were placed over an aluminum foil lined cooler containing dry ice. Frozen material was removed by with a mallet and sectioned into 10cm depth intervals from 0-60 cm (n = 6 per profile, except for N3 which was sectioned only from 30-60cm; total n = 33). The material was then wrapped in the foil and transported on dry ice to permanent storage at -80°OC.

Particle Size Distribution.

Samples were dried for 4-5 days at 105°OC, weighed, then transferred to 4L polypropylene Nalgene bottles and vigorously agitated to break up aggregates. Material was then sieved into1- phi size classes from 64mm (-6 phi) to <.062mm (5 phi) and weighed to determine the weight percentage for each fraction. Each subsample was placed in a 50ml Corning tube with 25ml of 1% pyrophosphate solution and placed on a rotary shaker overnight. This mixture was then poured and washed through a #230 sieve (.062mm). Material retained on the sieve was dried overnight and weighed to determine the weight percentage of the sand fraction, which was then subtracted from the initial 10g to determine the silt and clay fraction. These measurements are then averaged and the weight-by-size fractions of the original 10g were determined. We used the Modified Wentworth Scale to define the mud fraction as <.062mm (#230 sieve), the sand fraction as <2mm to .062 (passes #10 sieve, but retained on a #230), and the gravel fraction as >2mm (retained on #10 sieve) to 64mm.

Sample Processing.

Samples were transferred to an anaerobic glovebag with 95%N_2 and 5% H_2 (Coy Laboratory Products, Grass Lake, MI) and thawed on clean 2mm stainless steel sieves prior to processing. Samples were sieved and homogenized; and 20g was subsampled into a pre-weighed, pre-cleaned 40ml glass vial for Fe(II) analysis. The remaining <2mm sieved and >2mm bulk samples were removed from the glovebag. Subsamples were collected from the <2mm fraction for further analysis. Approximately 5g was transferred into a 40-mL borosilicate glass vial and stored at -80°C for analysis of OC chemistry (see below). An additional sample was taken for elemental analysis (OC, N) and remaining material was divided into 20g samples collected into 40-mL borosilicate glass vials and stored at -80°C.

Analytical methods.

We analyzed sample geochemistry with the following approaches. Total carbon (OC), nitrogen (N), and sulfur (S) were measured using an Elementar vario EL cube (Elementar Co.Germany). To analyze ammonia (NH_4^+), we extracted 2g sediment with 4mL 2M KCl for 1hr on a reciprocal shaker. Extracts were filtered (0.22 um) and NH_4 was measured with Hach Kit 2604545 (Hach, Loveland, Co). Fe(II) content was assessed by ferrozine assay[66]. Briefly, 1g sediment was extracted for 1hr with 10 mL 0.5N HCl with 200 rpm shaking in an anaerobic chamber and filtered through 0.22um PTFE syringe filters. One mL of filtrate and 1 mL Ferrozine were combined in a 1.5 mL, and fluorescence was measured at 562 nm to determine Fe(II) content. Total Fe was determined by inductively coupled plasma (ICP), and Fe(III) was calculated as the difference between Fe(II) and total Fe. All other ion concentrations were measured by ICP on 0.5N HCl extractions, as described above.

In addition, we assessed aerobic metabolism in each sample with a resazurin reduction assay, modified from Haggerty *et al.*[67]. We added 6ml of filtered river water from the Columbia River to four replicate 1 cc subsamples, taken with a cut-off syringe, from each depth. One replicate vial from each location was heat killed in a 90°C water bath for 1 hour, and cooled on ice to bring back to 4°C. Resazurin incubations were started by adding 200µl of 30µM resazurin to vials when cold, gently mixing and then incubating on an angle at 50rpm and 21°C. After 4hr, vials were weighed and 6mL acetonitrile (ACN) added to begin a 1hr extraction. After ACN addition, vials were sealed, vortexed and weighed again before being placed in a sonicator bath for 10min. After sonication, vials were put back on the 50rpm shaker. After a 1hr extraction, vials were vortexed and sand was allowed to settle. The screw cap was removed to allow extract to be drawn into a 5-mL syringe fitted with a 20G needle. Extracts were filtered with 33mm, 0.2µm syringe filters (PES, Millex by Millipore) into pre-labeled 12-mL amber vials (Thermoscientific) and stored at 4°C. The vial with the remaining sand was dried in a convection oven at 75 ^{o}C for at least 72 hrs then weighed. Fluorescence emission maxima for resazurin (630nm) and resorufin (585nm) were measured on resazurin sample extracts using a Horiba Fluorolog 3 fluorimeter. 2mL extract was added to 0.2mL 100mM HEPES (pH 8) in quartz cuvettes and fluorescence intensity quantified by comparison to resazurin and resorufin standards made up in ACN:H_2O (1:1).

FT-ICR-MS solvent extraction.

Three solvents—water (H_2O), methanol (CH_3OH, hereafter “MeOH”) and chloroform ($CHCl_3$)—with different polarities were used to sequentially extract different classes of organic

compounds from samples according to Tfaily et al.[10,11] Water extractions were preformed first, followed by MeOH and $CHCl_3$. Water is selective for carbohydrates with high O/OC ratios, amino-sugars and other labile polar compounds; MeOH is selective for compounds with relatively low O/OC ratios and finally $CHCl_3$ is selective for lipid-like compounds[10]. Extracts were prepared by adding 1 ml of solvent to 100 mg bulk soil and shaking in 2 mL capped glass vials for two hours on an Eppendorf Thermomixer. Samples were removed from the shaker and left to stand before spinning down and pulling off the supernatant to stop the extraction. The soil residue was dried with nitrogen gas to remove any residual solvent, and then the next solvent was added. The $CHCl_3$ and H_2O extracts were diluted in MeOH to improve ESI efficiency. SOC extraction efficiency was estimated to be around 15% measured using protocol developed by Tfaily et al.[10].

FT-ICR-MS data acquisition and analysis.

Ultrahigh resolution characterization of the three different extracts from each sample was carried out using a 12 Tesla Bruker SolariX Fourier transform ion cyclotron resonance (FT-ICR) mass spectrometer (MS) located at the Environmental Molecular Sciences Laboratory (EMSL) in Richland, WA, USA. Samples were injected directly into the mass spectrometer and the ion accumulation time was optimized for all samples to account for differences in OC concentration, so that all samples injected into the mass spectrometer had similar concertation. A standard Bruker electrospray ionization (ESI) source was used to generate negatively charged molecular ions. Samples were introduced to the ESI source equipped with a fused silica tube (30 μm i.d.) through an Agilent 1200 series pump (Agilent Technologies) at a flow rate of 3.0 μL min^{-1}. Experimental conditions were as follows: needle voltage, +4.4 kV; Q1 set to 50 *m*/*z*; and the

heated resistively coated glass capillary operated at 180 °OC. One hundred fourty-four individual scans were averaged for each sample and internally calibrated using an organic matter homologous series separated by 14 Da (–CH2 groups). The mass measurement accuracy was less than 1 ppm for singly charged ions across a broad *m*/*z* range (100-1200 *m*/*z*). The mass resolution was ~ 350K at 339 m/z. Data Analysis software (BrukerDaltonik version 4.2) was used to convert raw spectra to a list of m/z values applying FTMS peak picker with a signal-to-noise ratio (S/N) threshold set to 7 and absolute intensity threshold to the default value of 100. Chemical formulae were then assigned using in-house built software following the Compound Identification Algorithm (CIA), described by Kujawinski and Behn[68] and modified by Minor et al.[69]. Chemical formulae were assigned based on the following criteria: S/N >7, and mass measurement error <1 ppm, taking into consideration the presence of OC, H, O, N, S and P and excluding other elements.

To aid in the interpretation of the large data sets, the chemical character of thousands of features for each sample's ESI FTICR-MS spectrum was evaluated on van Krevelen diagrams. Compounds were plotted on the van Krevelen diagram on the basis of their molar H:OC ratios (y-axis) and molar O:OC ratios (x-axis). Van Krevelen diagrams provide a means to visualize and compare the average properties of OM and assign compounds to the major biochemical classes (*i.e.*, lipid-, protein-, lignin-, unsaturated hydrocarbon-, and condensed hydrocarbon-like). In this study, biochemical compound classes are reported as relative abundance values based on counts of OC, H, and O for the following H:OC and O:OC ranges; lipids ($0 < O:OC \leq 0.3$, $1.5 \leq H:OC \leq 2.5$), unsaturated hydrocarbons ($0 \leq O:OC \leq 0.125$, $0.8 \leq H:OC < 2.5$), proteins ($0.3 < O:OC \leq 0.55$, $1.5 \leq H:OC \leq 2.3$), amino sugars ($0.55 < O:OC \leq 0.7$, $1.5 \leq H:OC \leq 2.2$), lignin ($0.125 < O:OC \leq 0.65$, $0.8 \leq H:OC < 1.5$), tannins ($0.65 < O:OC \leq 1.1$, $0.8 \leq H:OC < 1.5$), and

condensed hydrocarbons ($0 \leq 200$ O:OC ≤ 0.95, $0.2 \leq$ H:OC < 0.8)[10]. To identify potential microbial transformation pathways, the mass difference between m/z peaks extracted from each spectrum with S/N>7 were compared to commonly observed mass difference for common metabolic transformations[70].

Statistical Methods.

All statistical analyses were conducted using R software (https://www.r-project.org/), and FT-ICR m/z intensities were converted into presence/absence data prior to analysis as per Kujawinski and Behn[68] and Minor et al.[69]. To examine differences in OC composition between transects, we constructed a Sorenson dissimilarity matrix for all m/z's identified (i.e., both assigned and unassigned peaks) within each OC pool ('vegan' package). Differences between transects were tested with PERMANOVA (999 permutations, 'vegan') and visualized using Non-metric Multidimensional Scaling (NMDS, 'vegan'). One sample (NR, profile 1, depth 30-40cm) was removed due to peak interference during FT-ICR-MS, and three samples (NR, profile 2, depths 00-10cm, 10-20cm, 20-30cm) were excluded because were unable to collect sufficient sample mass for all analyses.

Further, we inferred the biochemistry of OC oxidation at R vs. NR by correlating chemical transformations in each OC pool to rates of metabolism. Chemical transformations were identified as mass differences in known biochemical pathways between peaks detected by FT-ICR-MS (i.e., the mass gained or lost in reactions, see Fig. 2). The number of times each chemical transformations occurred in sample was summed and correlated to aerobic metabolism (resazurin assay) using Pearson's product-moment correlation coefficient. Positive relationships were inferred to denote possible processes of biotic OC oxidation. We also constructed Bray-

Curtis dissimilarity matrices of transformations that positively correlated with aerobic metabolism, visualized them by vegetation state with non-metric Multidimensional Scaling visualization (NMDS, 'vegan'), and statistically evaluated them with PERMANOVA (999 permutations, 'vegan').

We also assessed metabolic pathways associated with OC transformations by mapping each peak (i.e., m/z in FT-ICR-MS data) that positively correlated to aerobic metabolism to the Kyoto Encyclopedia of Genes and Genomes (KEGG, Release 80.0, http://www.kegg.jp)[31] using an in-house software. By doing so, we were able to assess the potential metabolic pathway that produced or utilized this particular compound and the potential Enzyme Commission number catalyzing this particular reaction. As per C transformations, we correlated the abundance of KEGG pathways to aerobic metabolism and inferred positive correlations as significant microbial microbial pathways contributing to OC oxidation. The number of times each positively correlated KEGG pathway occurred in each sample was normalized by the total number of pathways detected in the sample to yield data as a relative abundance. The normalized abundance of each pathway was clustered using hierarchical clustering and visualized using the 'pheatmap' package in R. Clusters were determined using the 'hclust' alogorithim in *R* with the 'complete linkage' clustering method.

Finally, we examined associations between aerobic metabolism, and thermodynamics by calculating the Gibbs Free Energy of OC oxidation (ΔG_{Cox}) from the Nominal Oxidation State of Carbon (NOSC) as per La Rowe and Van Cappellen[46]. NOSC is calculated from the number of electrons transferred in OC oxidation half reactions and is defined by the equation:

(1) $NOSC = -((-Z + 4a + b - 3c - 2d + 5e - 2f)/a) + 4$

, where a, b, c, d, e, and f are the stoichiometric numbers of elements OC, H, N, O, P, S in organic material and Z is net charge of organic compound. This method utilizes stoichiometric elemental ratios of organic matter to infer thermodynamics associated with OC half reactions and is determined from the equation:

$$(2)\ \Delta G_{Cox} = 60.3 - 28.5(NOSC)$$

Values of ΔG_{Cox} are generally positive, indicating that OC oxidation must be coupled to the reduction of a terminal electron acceptor for a thermodynamically favorable reaction, and higher ΔG_{Cox} denotes a less thermodynamically favorable compound. Here, we assessed relationships between aerobic metabolism and ΔG_{Cox} of OC compounds in each OC pool using linear regressions in each transect, in which aerobic metabolism was the independent variable and ΔG_{Cox} was the dependent variable.

Author Contributions.

EBG was responsible for conceptual development and data analysis and was the primary writer with guidance from JCS and MT. ARC, AEG, CTR, ECR, DWK, and JCS were responsible for experimental design and data collection. MT was responsible for all FT-ICR processing. All authors contributed to manuscript revisions.

Author Information.

Reprints and permissions information is available at www.nature.com/reprints. We declare no competing financial interests. Correspondence and requests for materials should be addressed to emily.graham@pnnl.gov.

Acknowledgements.

This research was supported by the US Department of Energy (DOE), Office of Biological and Environmental Research (BER), as part of Subsurface Biogeochemical Research Program's Scientific Focus Area (SFA) at the Pacific Northwest National Laboratory (PNNL). PNNL is operated for DOE by Battelle under contract DE-AC06-76RLO 1830. A portion of the research was performed at Environmental Molecular Science Laboratory User Facility.

Figure 1. NMDS visualization of dissimilarity in OC pool composition. Water-soluble and bound-OC pools are represented by open circles and x's, respectively. Samples associated with riparian vegetation are blue, and those in areas without vegetation are red. The P-value reflects differences among all groups, as assessed by PERMANOVA. Within each extraction, the composition of OC pools was significantly different across vegetation states (both P = 0.001).

Figure 2. Methodology for inferring biochemical transformations and metabolic pathways. (a) Biochemical OC transformations were calculated by identifying known mass transfers in biochemical transformations. For each transformation, the peaks (i.e., products and reactants) between which masses were transferred were mapped to metabolic (KEGG) pathways. (b) Biochemical transformations and metabolic pathways were then correlated to aerobic metabolism to garner insights into OC oxidation processes.

Figure 3. NMDS visualization of C transformation partitioning among transects. The identities of transformations that correlated to aerobic metabolism were significantly different among vegetation states in both the (a) water-soluble and (b) bound-OC pools. R and NR are denoted in blue and red, respectively, and significance values are derived from PERMANOVA.

Figure 4. KEGG pathways associated with aerobic metabolism. A hierarchical clustering heatmap shows KEGG pathways positively associated with aerobic metabolism. Colors move from white to red from a scale of 0% to 20%, showing percent relative abundance of each pathway in each group. Clusters were calculated using the 'complete linkage' method in the *R* command 'hclust'. Pathways are described and divided by cluster and listed in the legend. RW,

RC, NRW, and NRC are placed on branches that yield clusters with which they are predominantly associated.

Figure 5. Correlations between Gibbs Free Energy of carbon oxidation and aerobic metabolism. (a) and (b) display linear regressions between aerobic metabolism and the Gibbs Free Energy of Carbon Oxidation(ΔG_{Cox}) in water-soluble and bound-OC pools, respectively. R and NR are denoted in blue and red. Solid lines show significant relationships at R; dashed lines show significant relationships at NR.

Figure 6. Conceptualization of relationship between riparian vegetation and OC oxidation. We propose a conceptualization of OC oxidation at terrestrial-aquatic interfaces whereby (a) areas deplete in riparian vegetation experience lower inputs to water-soluble OC pools coincident with lower rates of oxidation. This results in overall smaller OC pools (both water-soluble and bound) and greater comparative oxidation of the bound-OC pool. Conversely, more riparian vegetation (b) results in greater terrestrial C deposition and larger water-soluble and bound-OC pools. However, water-soluble OC is preferentially oxidized, resulting in a more stabilized bound-OC pool. (b) In both cases, thermodynamically-favorable portions of OC pools are oxidized, but discrete OC pools are metabolized in the presence or absence of riparian vegetation. Boxes denote pool sizes, and the thickness of arrow denotes flux magnitude.

Table 1. Abbreviations and Acronyms.

Table 2. C transformations correlating with aerobic metabolism.

1 Burd, A. B. *et al.* Terrestrial and marine perspectives on modeling organic matter degradation pathways. *Global change biology* **22**, 121-136 (2016).

2 Todd-Brown, K. *et al.* Causes of variation in soil carbon simulations from CMIP5 Earth system models and comparison with observations. *Biogeosciences* **10** (2013).

3 Wieder, W. R., Bonan, G. B. & Allison, S. D. Global soil carbon projections are improved by modelling microbial processes. *Nature Climate Change* **3**, 909-912 (2013).

4 Wieder, W. R., Cleveland, C. C., Smith, W. K. & Todd-Brown, K. Future productivity and carbon storage limited by terrestrial nutrient availability. *Nature Geoscience* **8**, 441-444 (2015).

5 Battin, T. J. *et al.* The boundless carbon cycle. *Nature Geoscience* **2**, 598-600 (2009).

6 Aalto, R. *et al.* Episodic sediment accumulation on Amazonian flood plains influenced by El Nino/Southern Oscillation. *Nature* **425**, 493-497 (2003).

7 Battin, T. J. *et al.* Biophysical controls on organic carbon fluxes in fluvial networks. *Nature Geoscience* **1**, 95-100 (2008).

8 Regnier, P. *et al.* Anthropogenic perturbation of the carbon fluxes from land to ocean. *Nature geoscience* **6**, 597-607 (2013).

9 Mason, H., Begg, J., Maxwell, R. S., Kersting, A. B. & Zavarin, M. A novel solid-state NMR method for the investigation of trivalent lanthanide sorption on amorphous silica at low surface loadings. *Environmental Science: Processes & Impacts* (2016).

10 Tfaily, M. M. *et al.* Advanced solvent based methods for molecular characterization of soil organic matter by high-resolution mass spectrometry. *Analytical chemistry* **87**, 5206-5215 (2015).

11 Tfaily, M. M. *et al.* Sequential extraction protocol for organic matter from soils and sediments using high resolution mass spectrometry and proton NMR. (In review).

12 Schmidt, M. W. *et al.* Persistence of soil organic matter as an ecosystem property. *Nature* **478**, 49-56 (2011).

13 Hedges, J. & Oades, J. Comparative organic geochemistries of soils and marine sediments. *Organic geochemistry* **27**, 319-361 (1997).

14 Hedges, J. I. *et al.* The molecularly-uncharacterized component of nonliving organic matter in natural environments. *Organic Geochemistry* **31**, 945-958 (2000).

15 Kuzyakov, Y. Priming effects: interactions between living and dead organic matter. *Soil Biology and Biochemistry* **42**, 1363-1371 (2010).

16 Guenet, B., Danger, M., Abbadie, L. & Lacroix, G. Priming effect: bridging the gap between terrestrial and aquatic ecology. *Ecology* **91**, 2850-2861 (2010).

17 Bengtsson, M. M. *et al.* No evidence of aquatic priming effects in hyporheic zone microcosms. *Scientific reports* **4**, 5187 (2014).

18 Bianchi, T. S. The role of terrestrially derived organic carbon in the coastal ocean: A changing paradigm and the priming effect. *Proceedings of the National Academy of Sciences* **108**, 19473-19481 (2011).

19 Hunter, W. R. *et al.* Metabolism of mineral‐sorbed organic matter and microbial lifestyles in fluvial ecosystems. *Geophysical Research Letters* (2016).

20 Hedges, J. I. & Keil, R. G. Sedimentary organic matter preservation: an assessment and speculative synthesis. *Marine chemistry* **49**, 81-115 (1995).

21 Rothman, D. H. & Forney, D. C. Physical model for the decay and preservation of marine organic carbon. *Science* **316**, 1325-1328 (2007).

22 Dorado-García, I., Syväranta, J., Devlin, S. P., Medina-Sánchez, J. M. & Jones, R. I. Experimental assessment of a possible microbial priming effect in a humic boreal lake. *Aquatic Sciences* **78**, 191-202 (2016).

23 Catalán, N., Kellerman, A. M., Peter, H., Carmona, F. & Tranvik, L. J. Absence of a priming effect on dissolved organic carbon degradation in lake water. *Limnology and Oceanography* **60**, 159-168 (2015).

24 Cotrufo, M. F., Wallenstein, M. D., Boot, C. M., Denef, K. & Paul, E. The Microbial Efficiency‐Matrix Stabilization (MEMS) framework integrates plant litter decomposition with soil organic matter stabilization: do labile plant inputs form stable soil organic matter? *Global Change Biology* **19**, 988-995 (2013).

25 Lehmann, J. & Kleber, M. The contentious nature of soil organic matter. *Nature* **528**, 60-68 (2015).

26 Ebel, W. J., Becker, C. D., Mullan, J. W. & Raymond, H. L. The Columbia River--toward a holistic understanding. *Canadian special publication of fisheries and aquatic sciences/Publication speciale canadienne des sciences halieutiques et aquatiques. 1989.* (1989).

27 Moser, D. P. *et al*. Biogeochemical processes and microbial characteristics across groundwater-surface water boundaries of the Hanford Reach of the Columbia River. *Environmental Science & Technology* **37**, 5127-5134 (2003).

28 Graham, E. B. *et al.* Dissolved organic matter and inorganic mercury loadings favor novel methylators and fermentation metabolisms in oligotrophic sediments. *bioRxiv*, 072017 (2016).

29 Castle, S. C. *et al.* Biogeochemical drivers of microbial community convergence across actively retreating glaciers. *Soil Biology and Biochemistry* **101**, 74-84 (2016).

30 Foley, J. A. *et al.* Global consequences of land use. *science* **309**, 570-574 (2005).

31 Kanehisa, M. & Goto, S. KEGG: kyoto encyclopedia of genes and genomes. *Nucleic acids research* **28**, 27-30 (2000).

32 Agati, G., Azzarello, E., Pollastri, S. & Tattini, M. Flavonoids as antioxidants in plants: location and functional significance. *Plant Science* **196**, 67-76 (2012).

33 Tholl, D. in *Biotechnology of Isoprenoids* 63-106 (Springer, 2015).

34 Willaman, J. J. & Schubert, B. G. *Alkaloid-bearing plants and their contained alkaloids*. (Agricultural Research Service, US Department of Agriculture, 1961).

35 Trail, F., Mahanti, N. & Linz, J. Molecular biology of aflatoxin biosynthesis. *Microbiology* **141**, 755-765 (1995).

36 Hahlbrock, K. & Scheel, D. Physiology and molecular biology of phenylpropanoid metabolism. *Annual review of plant biology* **40**, 347-369 (1989).

37 Shepherd, T. & Wynne Griffiths, D. The effects of stress on plant cuticular waxes. *New Phytologist* **171**, 469-499 (2006).

38 Raffaele, S., Leger, A. & Roby, D. Very long chain fatty acid and lipid signaling in the response of plants to pathogens. *Plant signaling & behavior* **4**, 94-99 (2009).

39 King, A., Nam, J.-W., Han, J., Hilliard, J. & Jaworski, J. G. Cuticular wax biosynthesis in petunia petals: cloning and characterization of an alcohol-acyltransferase that synthesizes wax-esters. *Planta* **226**, 381-394 (2007).

40 Crawford, M. *et al.* Role of plant-derived omega–3 fatty acids in human nutrition. *Annals of Nutrition and Metabolism* **44**, 263-265 (2000).

41 Creelman, R. A. & Mulpuri, R. The oxylipin pathway in Arabidopsis. *The Arabidopsis Book*, e0012 (2002).

42 Bishop, G. J. Refining the plant steroid hormone biosynthesis pathway. *Trends in plant science* **12**, 377-380 (2007).

43 Hedin, L. O. *et al.* Thermodynamic constraints on nitrogentransformations and other biogeochemicalprocesses at soil–stream interfaces. *Ecology* **79**, 684-703 (1998).

44 Burgin, A. J., Yang, W. H., Hamilton, S. K. & Silver, W. L. Beyond carbon and nitrogen: how the microbial energy economy couples elemental cycles in diverse ecosystems. *Frontiers in Ecology and the Environment* **9**, 44-52 (2011).

45 Helton, A. M., Ardón, M. & Bernhardt, E. S. Thermodynamic constraints on the utility of ecological stoichiometry for explaining global biogeochemical patterns. *Ecology letters* **18**, 1049-1056 (2015).

46 LaRowe, D. E. & Van Cappellen, P. Degradation of natural organic matter: a thermodynamic analysis. *Geochimica et Cosmochimica Acta* **75**, 2030-2042 (2011).

47 Blagodatskaya, E. & Kuzyakov, Y. Mechanisms of real and apparent priming effects and their dependence on soil microbial biomass and community structure: critical review. *Biology and Fertility of Soils* **45**, 115-131 (2008).

48 Fang, J. *et al.* Precipitation patterns alter growth of temperate vegetation. *Geophysical research letters* **32** (2005).

49 Knapp, A. K. *et al.* Consequences of more extreme precipitation regimes for terrestrial ecosystems. *Bioscience* **58**, 811-821 (2008).

50 Smith, R. M. & Kaushal, S. S. Carbon cycle of an urban watershed: exports, sources, and metabolism. *Biogeochemistry* **126**, 173-195 (2015).

51 Imberger, S. J., Thompson, R. M. & Grace, M. R. Urban catchment hydrology overwhelms reach scale effects of riparian vegetation on organic matter dynamics. *Freshwater Biology* **56**, 1370-1389 (2011).

52 Fraley, L. M., Miller, A. J. & Welty, C. Contribution of In‐Channel Processes to Sediment Yield of an Urbanizing Watershed1. *JAWRA Journal of the American Water Resources Association* **45**, 748-766 (2009).

53 Graeber, D., Gelbrecht, J., Pusch, M. T., Anlanger, C. & von Schiller, D. Agriculture has changed the amount and composition of dissolved organic matter in Central European headwater streams. *Science of the Total Environment* **438**, 435-446 (2012).

54 Larson, J. H. *et al.* Relationships between land cover and dissolved organic matter change along the river to lake transition. *Ecosystems* **17**, 1413-1425 (2014).

55 Six, J. *et al.* Measuring and understanding carbon storage in afforested soils by physical fractionation. *Soil science society of America journal* **66**, 1981-1987 (2002).

56 Zachara, J. M. *et al.* Persistence of uranium groundwater plumes: Contrasting mechanisms at two DOE sites in the groundwater–river interaction zone. *Journal of Contaminant Hydrology* **147**, 45-72 (2013).

57 Slater, L. D. *et al.* Use of electrical imaging and distributed temperature sensing methods to characterize surface water–groundwater exchange regulating uranium transport at the Hanford 300 Area, Washington. *Water Resources Research* **46** (2010).

58 Graham, E. B. *et al.* Coupling spatiotemporal community assembly processes to changes in microbial metabolism. *Frontiers in Microbiology* **7**, 1949 (2016).

59 Lin, X. *et al.* Spatial and temporal dynamics of the microbial community in the Hanford unconfined aquifer. *The ISME Journal* **6**, 1665-1676 (2012).

60 Stegen, J. C., Lin, X., Konopka, A. E. & Fredrickson, J. K. Stochastic and deterministic assembly processes in subsurface microbial communities. *The ISME Journal* **6**, 1653-1664 (2012).

61 Arntzen, E. V., Geist, D. R. & Dresel, P. E. Effects of fluctuating river flow on groundwater/surface water mixing in the hyporheic zone of a regulated, large cobble bed river. *River Research and Applications* **22**, 937-946 (2006).

62 Peterson, R. E. & Connelly, M. P. Water movement in the zone of interaction between groundwater and the Columbia River, Hanford site, Washington. *Journal of Hydraulic Research* **42**, 53-58 (2004).

63 Stegen, J. C. *et al.* Groundwater-surface water mixing shifts ecological assembly processes and stimulates organic carbon turnover. *Nature Communications* **7** (2016).

64 Lotspeich, F. B. & Reid, B. H. Tri-tube freeze-core procedure for sampling stream gravels. *The Progressive Fish-Culturist* **42**, 96-99 (1980).

65 Rood, K. & Church, M. Modified freeze-core technique for sampling the permanently wetted streambed. *North American Journal of Fisheries Management* **14**, 852-861 (1994).

66 Stookey, L. L. Ferrozine---a new spectrophotometric reagent for iron. *Analytical chemistry* **42**, 779-781 (1970).

67 Haggerty, R., Martí, E., Argerich, A., Von Schiller, D. & Grimm, N. B. Resazurin as a "smart" tracer for quantifying metabolically active transient storage in stream ecosystems. *Journal of Geophysical Research: Biogeosciences* **114** (2009).

68 Kujawinski, E. B. & Behn, M. D. Automated analysis of electrospray ionization Fourier transform ion cyclotron resonance mass spectra of natural organic matter. *Analytical Chemistry* **78**, 4363-4373 (2006).

69 Minor, E. C., Steinbring, C. J., Longnecker, K. & Kujawinski, E. B. Characterization of dissolved organic matter in Lake Superior and its watershed using ultrahigh resolution mass spectrometry. *Organic Geochemistry* **43**, 1-11 (2012).

70 Breitling, R., Ritchie, S., Goodenowe, D., Stewart, M. L. & Barrett, M. P. Ab initio prediction of metabolic networks using Fourier transform mass spectrometry data. *Metabolomics* **2**, 155-164 (2006).

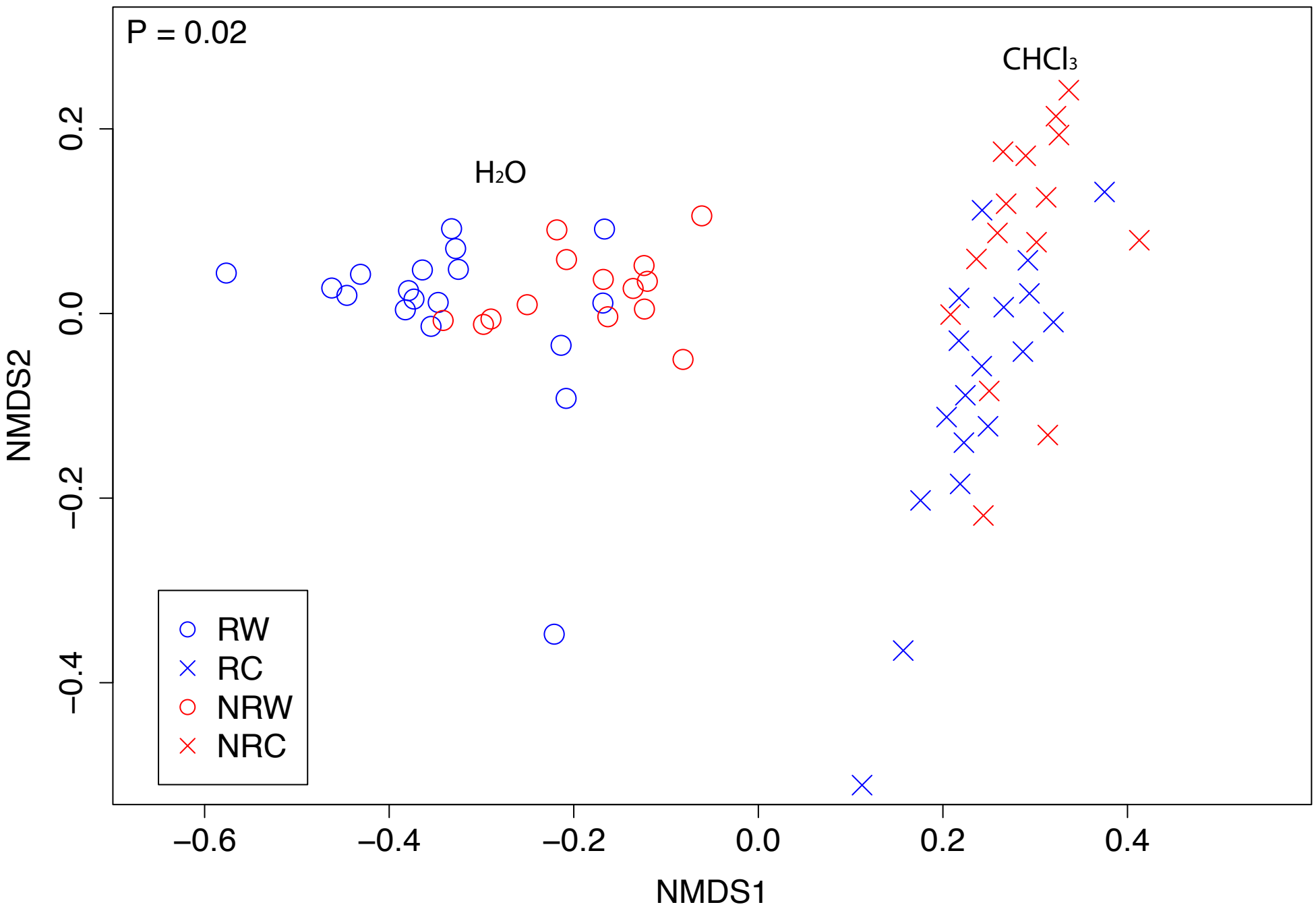
P = 0.02
CHCl3
H2O
RW
RC
NRW
NRC
NMDS2
NMDS1
0.2
0.0
−0.2
−0.4
−0.6
−0.4
−0.2
0.0
0.2
0.4

a

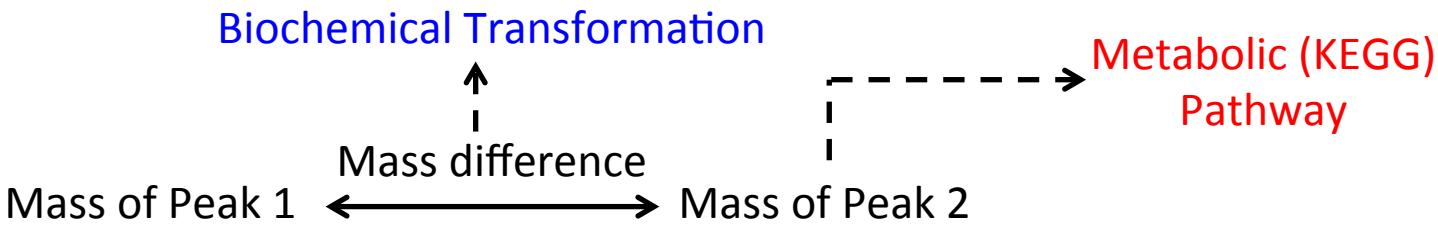
Biochemical Transformation
Metabolic (KEGG) Pathway
Mass difference
Mass of Peak 1
Mass of Peak 2

b

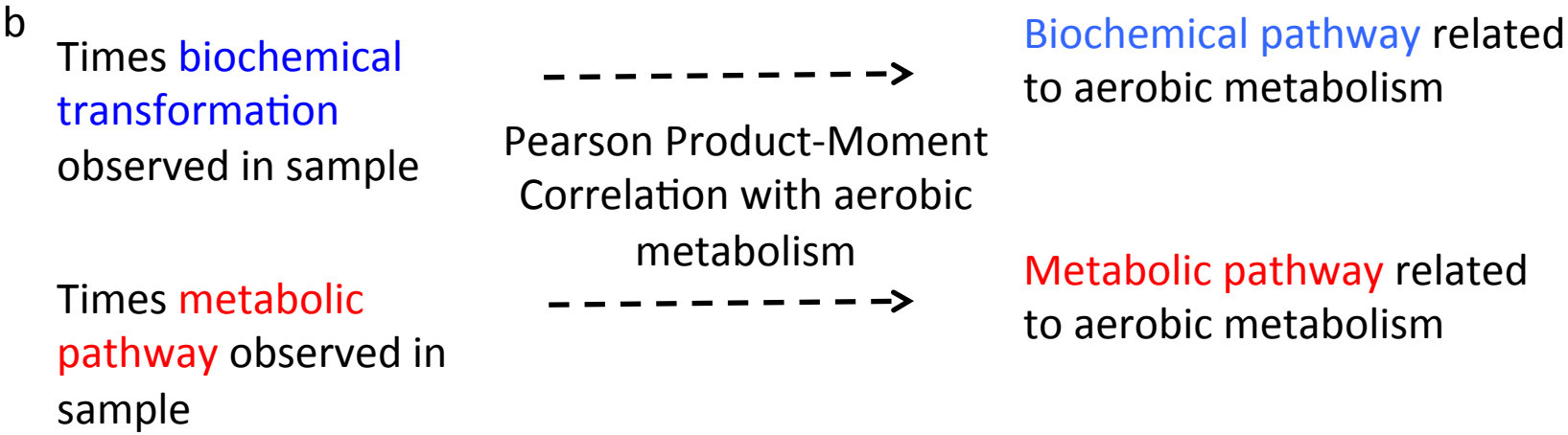
Times biochemical transformation observed in sample
Biochemical pathway related to aerobic metabolism
Pearson Product-Moment Correlation with aerobic metabolism
Times metabolic pathway observed in sample
Metabolic pathway related to aerobic metabolism

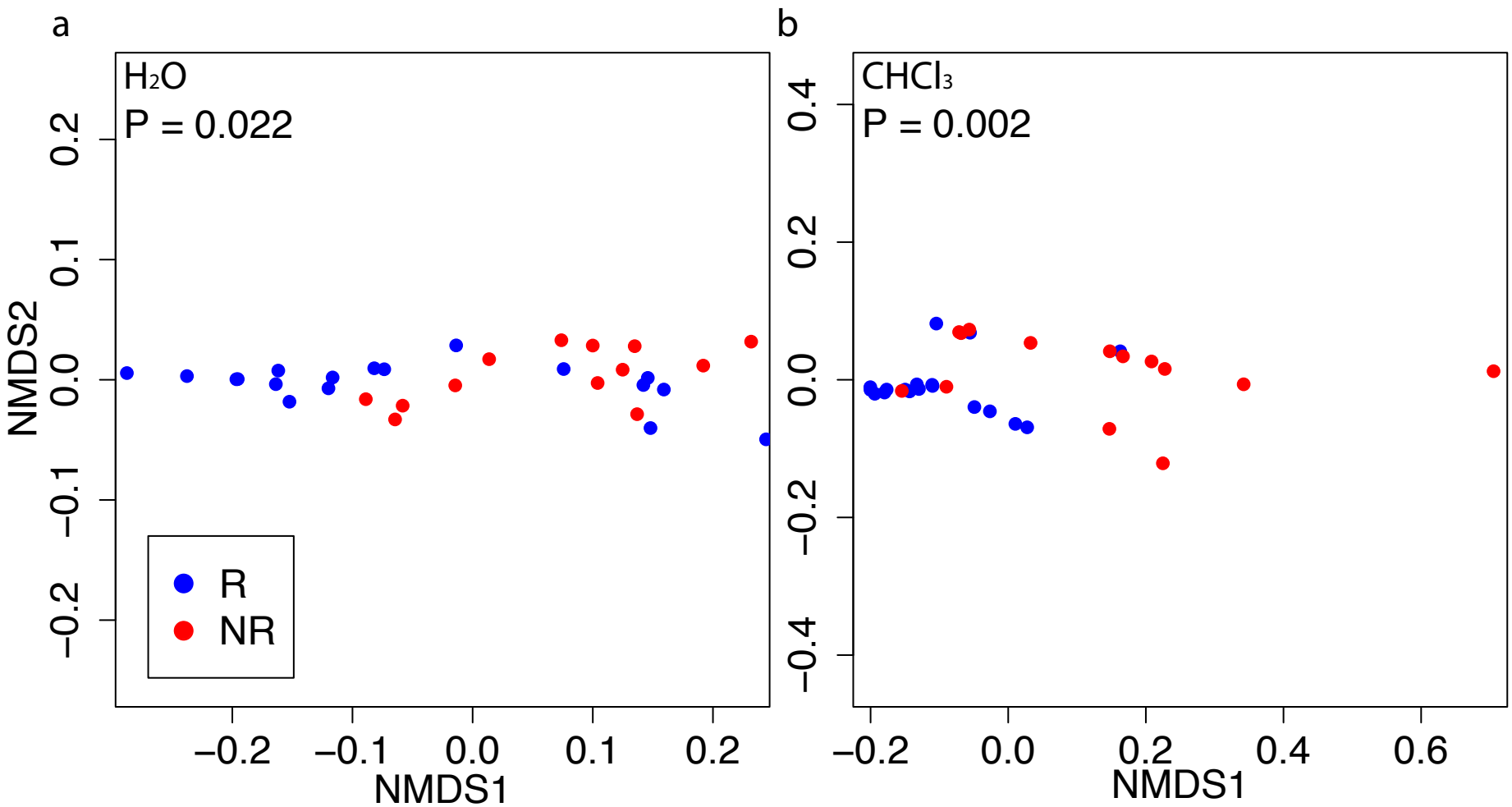
a
H2O
P = 0.022
NMDS2
0.2
0.1
0.0
−0.1
−0.2
R
NR
−0.2
−0.1
0.0
0.1
0.2
NMDS1
b
CHCl3
P = 0.002
0.4
0.2
0.0
−0.2
−0.4
−0.2
0.0
0.2
0.4
0.6
NMDS1

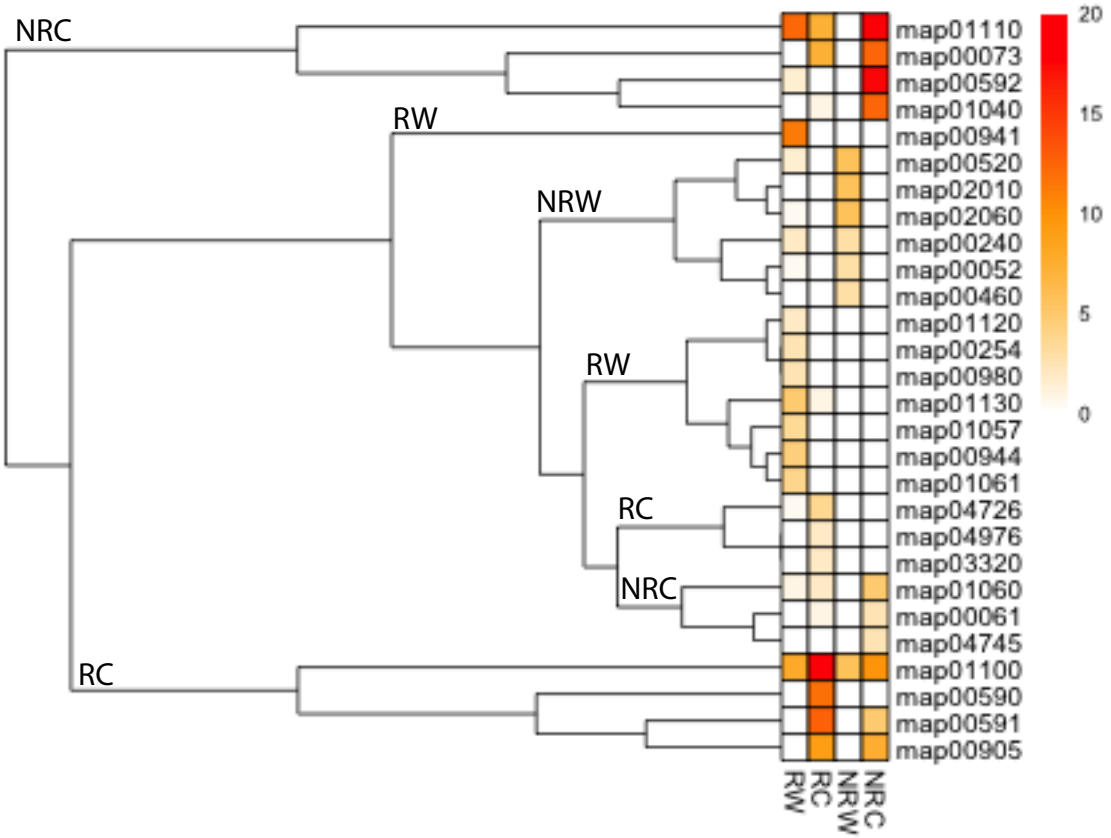

	Pathway	Pathway Description
Cluster 1	map01110	Biosynthesis of secondary metabolites
	map00073	Cutin, suberine and wax biosynthesis
	map00592	alpha-Linolenic acid metabolism
	map01040	Biosynthesis of unsaturated fatty acids
Cluster 2	map00941	Flavonoid biosynthesis
Cluster 3	map00520	Amino sugar and nucleotide sugar metabolism
	map02010	ABC transporters
	map02060	Phosphotransferase system (PTS)
	map00240	Pyrimidine metabolism
	map00052	Galactose metabolism
	map00460	Cyanoamino acid metabolism
Cluster 4	map01120	Microbial metabolism in diverse environments
	map00254	Aflatoxin biosynthesis
	map00980	Metabolism of xenobiotics by cytochrome P450
	map01130	Biosynthesis of antibiotics
	map01057	Biosynthesis of type II polyketide products
	map00944	Flavone and flavonol biosynthesis
	map01061	Biosynthesis of phenylpropanoids
Cluster 5	map04726	Serotonergic synapse
	map04976	Bile secretion
	map03320	PPAR signaling pathway
Cluster 6	map01060	Biosynthesis of plant secondary metabolites
	map00061	Fatty acid biosynthesis
	map04745	Phototransduction - fly
Cluster 7	map01100	Metabolic pathways
	map00590	Arachidonic acid metabolism
	map00591	Linoleic acid metabolism
	map00905	Brassinosteroid biosynthesis

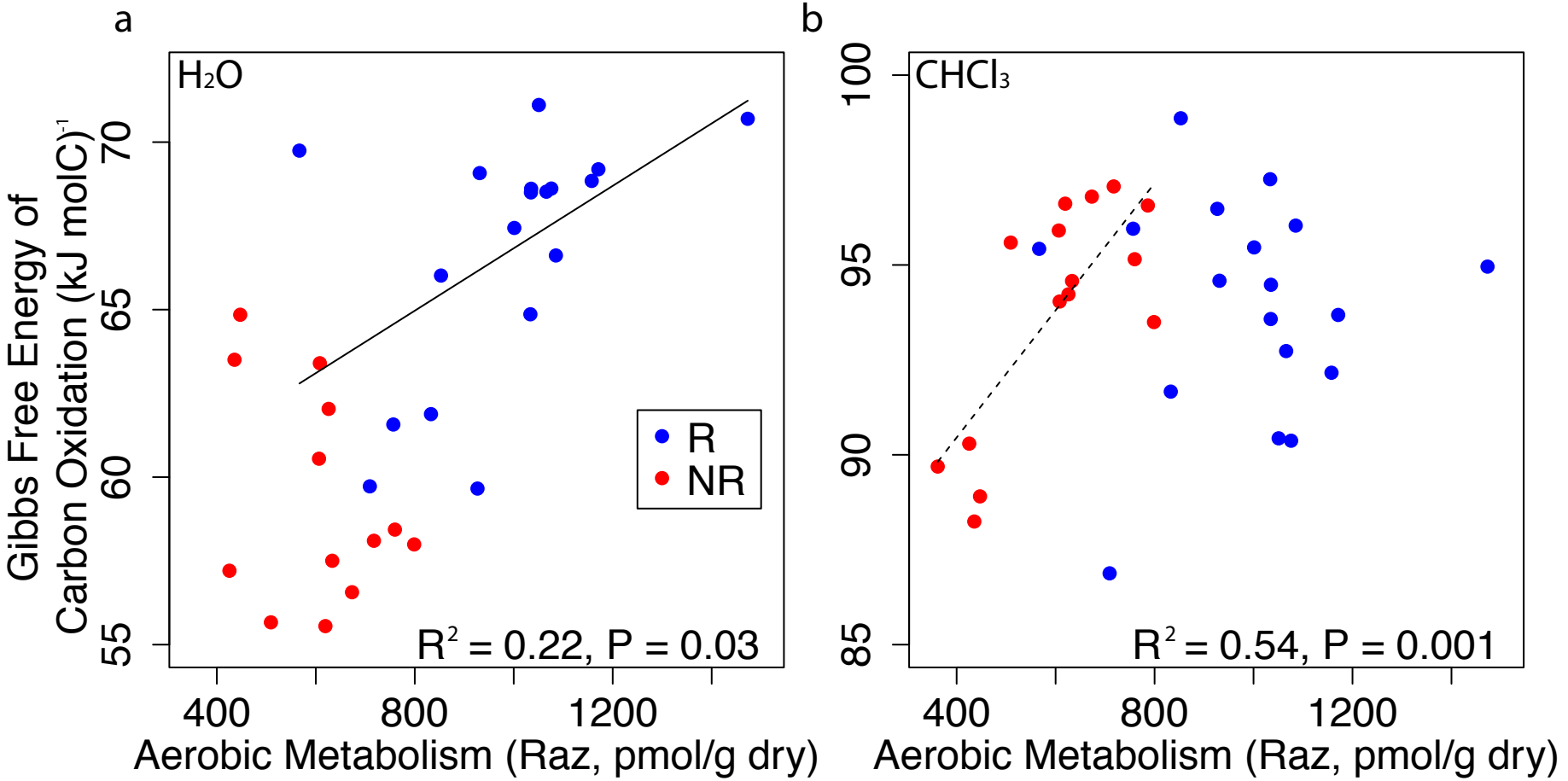
a
b
H2O
CHCl3
Gibbs Free Energy of Carbon Oxidation (kJ molC)-1
55
60
65
70
85
90
95
100
400
800
1200
Aerobic Metabolism (Raz, pmol/g dry)
R
NR
R2 = 0.22, P = 0.03
R2 = 0.54, P = 0.001

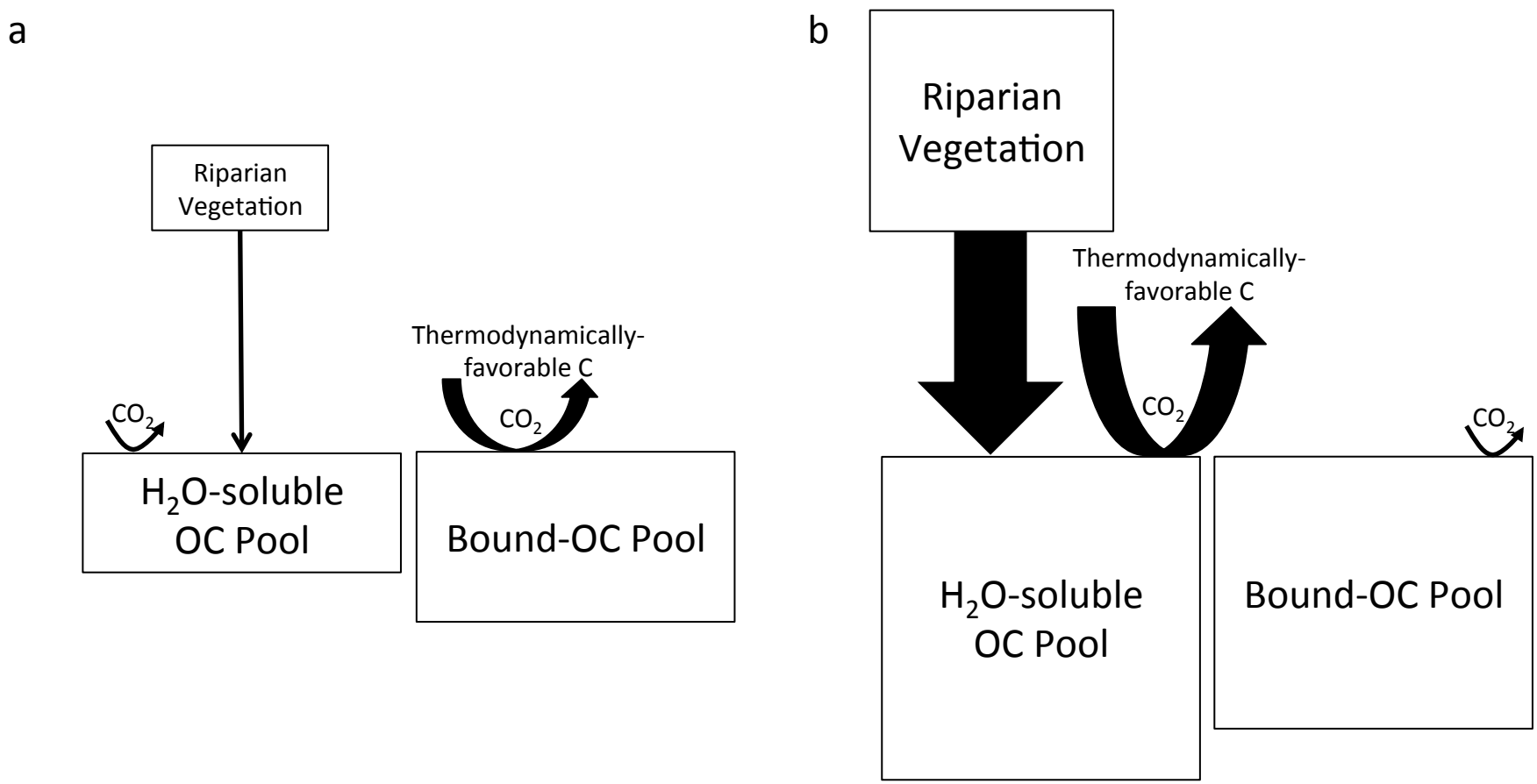
a
Riparian Vegetation
Thermodynamically-favorable C
CO_2
CO_2
H_2O-soluble OC Pool
Bound-OC Pool
b
Riparian Vegetation
Thermodynamically-favorable C
CO_2
CO_2
H_2O-soluble OC Pool
Bound-OC Pool

Abbreviation/Acronym	Description
R	Transect with dense riparian vegetation
NR	Transect with sparse riparian vegetation
RW	Transect R, water extraction
RC	Transect R, chloroform extraction
NRW	Transect NR, water extraction
NRC	Transect NR, chloroform extraction
H_2O	Water
$CHCl_3$	Chloroform
C	Carbon
OC	Organic carbon
FT-ICR-MS	Fourier transform ion cyclotron resonance mass spectrometry
KEGG	Kyoto Encyclopedia of Genes and Genomes
ΔG_{Cox}	Gibbs Free Energy of C oxidation

	Pearson's r
RW	
biotinyl_(-H)_C10H15N2O3S	0.74
uridine_5_diphosphate_(-H2O)_C9H12N2O11P2	0.67
cytosine_(-H)_C4H4N3O	0.65
uridine_5_monophosphate_(-H2O)_C9H11N2O8P	0.65
guanine_(-H)_C5H4N5O	0.61
guanosine_(-H2O)_C10H11N5O4	0.59
adenine_(-H)_C5H4N5	0.59
glutathione_(-H2O)_C10H15N3O5S	0.57
uracil_(-H)_C4H3N2O2	0.56
glucose_C6H12O6	0.53
C6H10O6	0.53
Aspartic_Acid_C4H5NO3	0.52
Glucuronic Acid (-H2O)	0.52
Lysine_C6H12N2O	0.51
D-Ribose (-H2O) (ribosylation)	0.50
secondary amine	0.50
Alanine_C3H5NO	0.50
C6H10O5	0.49
monosaccharide (-H2O)	0.49
Threonine_C4H7NO2	0.49
Glutamic_Acid_C5H7NO3	0.48
pentose_C5H8O4	0.47
acetotacetate_(-H2O)_C4H4O2	0.47
Glutamine_C5H8N2O2	0.47
pyridoxal_phosphate_(-H2O)_C8H8NO5P	0.47
RC	
isoprene_addition_(-H)_C5H7	0.61
phosphate	0.56
primary amine	0.55
Glucuronic Acid (-H2O)	0.53
glyoxylate_(-H2O)_C2O2	0.53
malonyl_group_(-H2O)_C3H2O3	0.52
D-Ribose (-H2O) (ribosylation)	0.49
pyrophosphate	0.49
acetotacetate_(-H2O)_C4H4O2	0.49
hydrogenation_dehydrogenation_H2	0.47
NRW	
NONE	NA
NRC	
Adenosine_5_monophosphate_(-H2O)_C10H12N5O6P	0.92
adenylate_(-H2O)_C10H12N5O6P	0.92
pyridoxal_phosphate_(-H2O)_C8H8NO5P	0.73
acetylation_(-H2O)_C2H2O	0.70
ketol group (-H2O)	0.70
Isoleucine_C6H11NO	0.69
Leucine_C6H11NO	0.69
ethyl addition_(-H2O)_C2H4	0.69
Threonine_C4H7NO2	0.69
Valine_C5H9NO	0.68
Carboxylation_CO2	0.68
Glycine_C2H3NO	0.67
Formic Acid_(-H2O)_CO	0.67
Serine_C3H5NO2	0.67
hydroxylation_(-H)_O	0.67
palmitoylation_(-H2O)_C16H30O	0.67
pentose_C5H8O4	0.66
secondary amine	0.66
condensation/dehydration_H2O	0.66
C2H2_C2H2	0.66
erythose (-H2O)	0.66
CH4_O	0.65
methanol (-H2O)	0.65
glyoxylate_(-H2O)_C2O2	0.65
NH_CH2	0.64
Alanine_C3H5NO	0.63
acetotacetate_(-H2O)_C4H4O2	0.63
Proline_C5H7NO	0.62
hydrogenation_dehydrogenation_H2	0.61
Histidine_C6H7N3O	0.60
malonyl_group_(-H2O)_C3H2O3	0.59
Cysteine_C3H5NOS	0.58
glcnac_C8H13N1O5	0.57
Methionine_C5H9NOS	0.57
Arginine_C6H12N4O	0.56
Aspartic_Acid_C4H5NO3	0.56
D-Ribose (-H2O) (ribosylation)	0.55